Localization and length-scale doubling in disordered films on soft substrates

Matthew R. Semler,[1] John M. Harris,[1] Andrew B. Croll,[1,*] and Erik K. Hobbie[1,2,*]
[1]*Department of Physics, North Dakota State University, Fargo, North Dakota 58108, USA*
[2]*Department of Coatings and Polymeric Materials, North Dakota State University, Fargo, North Dakota 58108, USA*
(Received 17 July 2013; revised manuscript received 10 August 2013; published 30 September 2013)

Wrinkling and folding are examined experimentally for three distinct types of disordered films on polydimethylsiloxane (PDMS) substrates; diblock copolymers, glassy polymers, and single-wall carbon nanotubes. All three of these systems exhibit localization and length-scale doubling at small strains, and we qualitatively account for these observations with a simple physical argument related to the width of the stress correlation function and the interaction of localization sites. Our results have relevance to wrinkling and folding in a diverse array of disordered films on soft substrates, and the insights offered here should help guide the development of theoretical models for the influence of structural disorder on thin-film wrinkling instabilities.

DOI: 10.1103/PhysRevE.88.032409 PACS number(s): 68.08.−p, 46.25.−y, 68.60.Bs, 81.05.Lg

I. INTRODUCTION

Thin films and coatings derived from complex materials are both ubiquitous in nature and of tremendous technological importance, and the deformation and durability of such films are topics of considerable interest [1–4]. In this regard, a significant body of recent work has focused on the surface wrinkling instabilities that emerge when a thin film resting on an elastic or viscous foundation is subjected to an in-plane compressive stress [5–12]. On an elastic substrate, such a coating undergoes a transition with increasing strain (ϵ) in which the film eventually buckles above a critical strain, ϵ_c. A balance of film bending and substrate stretching favors the formation of a periodic pattern, with a wavelength that has a simple and utilitarian relationship to the mechanical properties of the adhered film.

Like many linear models, this formalism has been applied with remarkable success well beyond the formal range of its validity, yet the large-strain (nonlinear) regime is nonetheless of considerable practical importance and represents an emerging area of research in thin-film mechanics [13–19]. Two themes of interest are "focusing" or localization [20–24], whereby the deformation becomes strongly heterogeneous, and doubling or bifurcation, where the characteristic length scale doubles with increasing strain [15,19]. Many studies have considered localization from a purely geometric point of view, but it is easy to show that geometric nonlinearity is not the only type of nonlinearity that can lead to localization, and in fact localization often leads to material failure in the form of banding, fracture, crazing, or delamination [25–28].

While most of the emphasis has been on wrinkling in structurally homogenous films, a number of practically relevant coatings can exhibit structural disorder and inhomogeneity over a broad range of length scales. These are, most notably, films cast from complex fluids composed of polymers, nanotubes, and colloids. Such materials can also exhibit power-law "thinning" or "softening", whereby the moduli decrease markedly with increasing strain or strain rate.

In this contribution, wrinkling and folding are examined experimentally for three seemingly unrelated examples of thin disordered films on polydimethylsiloxane (PDMS) substrates; diblock copolymers, glassy polymers, and single-wall carbon nanotubes. All three of these coatings are technologically important, and as we demonstrate here, all three exhibit localization and length-scale doubling at small strains. Although several recent papers have observed localization and/or bifurcation (most often in the context of large strains and material nonlinearity), material heterogeneity has rarely been considered in the analysis [29]. To qualitatively account for these observations, we offer a simple physical argument related to the width, interaction and spacing of localization triggered by defects. Our approach offers an empirical and intuitive picture of small-strain localization and length-scale doubling that has relevance to a broad range of disordered films on soft substrates.

II. EXPERIMENTS

We first experimentally examine the structural stability of thin disordered films cast from three different materials; diblock copolymers, glassy polymers, and single-wall carbon nanotubes. We consider these three specific examples below, focusing on the nature of the inhomogeneities and the onset of localization and doubling at small strains.

A. Diblock copolymers

Recent work with thin block-copolymer films reveals an interesting class of localized buckling triggered by controlled variations in film thickness [29]. Block copolymers are a surfactant like class of self-assembling materials comprised of two chemically distinct polymers joined at one end. The two polymers will phase separate if they are sufficiently dissimilar, but the bond between the two blocks frustrates the phase separation, which is then arrested on a length scale proportional to the length of the two blocks. In the bulk, the result is one of many intricate microstructures, determined primarily by the ratio of block lengths and the energetic cost of the interface [30]. A particularly simple lamellar morphology emerges when both blocks have similar lengths, since no intrinsic curvature is favored. When confined to a thin film,

*corresponding authors: andrew.croll@ndsu.edu; erik.hobbie@ndsu.edu

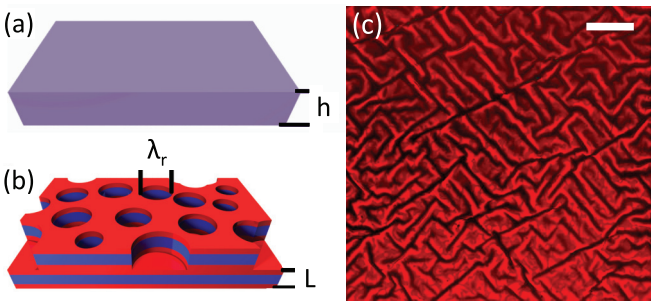

FIG. 1. (Color online) (a) Schematic of a spincast diblock copolymer film, and (b) the same film after microphase separation. The PDMS substrate is not shown, red/light represents the PS block, and blue/dark represents the P2VP block. The film thickness h is not commensurate with the lamellar spacing, L. (c) A typical laser scanning confocal microscope (LSCM) image of an equibiaxially stressed block copolymer film on PDMS (20 μm scale).

the lamellar state is faced with a challenge; the film thickness is not typically an integer multiple of lamellae. This constraint can only be satisfied when the topmost layer is incomplete, and the result is surface roughness exactly one lamellae in amplitude (Fig. 1).

The ability to finely tune surface roughness makes the diblock system ideal for exploring the influence of inhomogeneities on wrinkling. When a thin block copolymer film on a soft substrate is compressed, it will form either "harmonic" wrinkles (as in a homogeneous film) or localized "folds", depending on the dominant Fourier component of the surface roughness, λ_r. If λ_r is small, the film forms wrinkles just like a homogeneous film of the average thickness (h) which we refer to as "homogeneous" wrinkling [6]. This scenario is well-studied, and the wavelength of the harmonic deformation is

$$\lambda_0 = 2\pi h \left(\frac{\bar{E}}{3\bar{E}_s}\right)^{1/3}, \tag{1}$$

where $\bar{E} = E/(1-\nu^2)$ is the plane-strain modulus of the film or substrate (subscript s) and ν is the Poisson ratio [6]. When λ_r is large, the film wrinkles independently in thick and thin regions in accordance with Eq. (1), where h is then the respective mean thickness of the corresponding regions. If λ_r is similar to λ_0, however, the film focuses the deformation into localized folds, which can be a dramatic effect when the amplitude of the roughness is large [29]. The spacing between such folds has been measured to be twice the 'homogeneous' wavelength over more than a decade in λ_0, implying that the relation

$$\langle\lambda\rangle = 4\pi h \left(\frac{\bar{E}}{3\bar{E}_s}\right)^{1/3} \tag{2}$$

can be used to determine the modulus of the film from the mean spacing of folds, where h is again the mean thickness [29]. When the roughness is removed, the film wrinkles homogeneously in accordance with Eq. (1).

Here, we offer new experimental data with a reduced strength of the thickness fluctuations, $\delta h(\mathbf{r})$. In particular, we use polystyrene-b-poly(2-vinylpyridine) (PS-b-P2VP, 80 kg/mol, Polymer Source, Dorval) and spin coat films

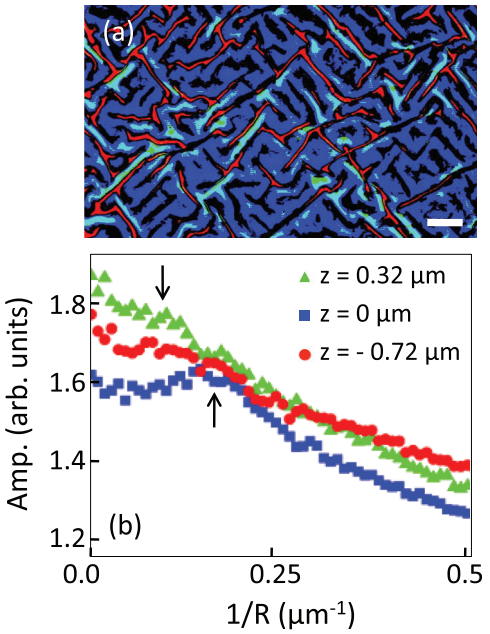

FIG. 2. (Color online) (a) An overlay of threshold images of single optical slices 320 nm above the average surface of the film (peaks—green/white), at the average surface (wrinkles—blue/gray), and 720 nm below the average surface (valleys—red/light gray, 10 μm scale). (b) Radially averaged FFT highlighting the different average spacing between wrinkles (blue squares), peaks (green triangles), and valleys (red circles), where the arrows indicate the location of peaks. The spacing of peaks and valleys is roughly twice that of the wrinkle spacing. All of the data are for the sample depicted in Fig. 1 as described in the text.

of approximately 160 nm thickness from toluene. The films are transferred to PDMS elastomer substrates (Dow Corning Sylgard 182), annealed at 140 °C and then quenched to room temperature (25 °C). The thermal mismatch between the film and the substrate imparts an equibiaxial compressive stress on the film, and the smallness of this stress ensures that the film is well within the linear-elastic regime. Annealing also allows lamellar layers to form with a period of $L = 48$ nm, and the surface breaks up to accommodate the incommensurability between the spincast thickness and the preferred lamellar spacing. The result is roughness of 48 nm on a 145 nm thick film. Again, localization only occurs when the roughness has a Fourier component similar to the homogeneous wavelength. Because the amplitude of the roughness is small, the effect is not as pronounced as in Ref. [29]. The wrinkling amplitude, however, is far from uniform, as evidenced in Fig. 2 through confocal microscopy. Fourier analysis reveals that the difference between the two length scales is again a factor of 2.

There are two important things to note here. First, the amplitude is being driven into a period doubling mode by noise, in agreement with what was demonstrated in a previous publication [29]. Second, the effect can only be related to the roughness of the copolymer film. This is because the films are initially flat after the spin-coating step, and they can be compressed and buckled in this as-spin-cast (non-lamellar) state to yield ordinary biaxial "harmonic" wrinkling. Only when microphase separation has occurred and the film has developed roughness can the doubling be triggered.

Furthermore, doubling is only realized when the roughness has a characteristic frequency similar to the "harmonic" wrinkling wavelength of the homogeneous film. Finally, the applied thermal stresses are very small (the thermal mismatch is 2.2×10^{-4} K^{-1}, meaning a quench of 100 K yields a strain of $\sim$2%), which rules out other possible nonlinearities [19].

B. Glassy polymers

Thin homopolymer films can exhibit a similar type of small-strain behavior, but the subtle interplay between quenched noise, film thickness, and strain in a glassy elastic film can give rise to more complex behavior. Here, polystyrene films (PS, 192 kg/mol, Sigma-Aldrich) were spun cast from toluene onto treated mica, floated on purified DI water, and then retrieved on both stretched PDMS for compression experiments and clean silicon wafers for characterizing unperturbed films. The films were annealed for 1 hour above the glass transition at $T = 110\,^{\circ}$C to promote compliance to the substrate, and the pre and post-wrinkling topography was studied using reflection optical microscopy and atomic-force microscopy (AFM). Figure 3 shows how regions of pure harmonic wrinkling coexist with regions of localization in compressed PS films on PDMS. For the longer wavelength patterns, the spacing qualitatively coincides with higher multiples of the measured pure wrinkling harmonic, λ_0. The modulus deduced from λ_0 via Eq. (1) is 2 GPa, in reasonable agreement with anticipated values [28].

More quantitatively, Fig. 4 shows the correlation function $c(\mathbf{r}) = \langle u(\mathbf{r})u(0)\rangle$ computed from such images for varied mean PS thickness at 5% strain. The projection along the strain (x) direction is shown in the lower panel. The measured fundamental wavelength λ_0, $2\lambda_0$, and $4\lambda_0$ are indicated as red hatch marks on the x axis. Interestingly, the prominent nearest-neighbor peak in $c(x)$ occurs at $x = 4\lambda_0$ instead of λ_0 or $2\lambda_0$. Since $c(x)$ is weighted by pixel intensity—which provides an approximate measure of the deformation amplitude $u(\mathbf{r})$—this implies that under certain conditions the dominant folds have an average spacing of $4\lambda_0$ rather than $2\lambda_0$ or λ_0. For the strains of interest here ($\epsilon \leqslant 10\%$), nonlinear elastic effects will be negligibly small [13].

Figure 5(a) shows an AFM image of the topography of an unstrained PS film (light) on PDMS (dark), and Fig. 5(b) shows thickness fluctuations obtained from projections of AFM images for unstrained films on both silicon (solid) and PDMS (dashed). The inset to Fig. 5(b) shows the digital structure factor, $S(q)$, for film roughness on PDMS, with a Gaussian fit giving the correlation length $\xi = 8.2\ \mu$m. Figure 5(c) shows an AFM image of the topography of a compressed film on PDMS with a projection along the direction of strain (shown in red/dark with the indicated scale). We note that surface roughness can originate from either thickness fluctuations in the film or roughness in the underlying surface of the PDMS. For the latter, the disorder then takes the form of quenched deformation imposed on the film prior to the application of strain. Although the PS films are smooth on silicon, the films on rubber are rough due to the underlying roughness of the PDMS. The amplitude of the fluctuations is comparable in magnitude to h and the length scale is comparable to or above λ_0, which can be identified as the smallest spacing in Fig. 3.

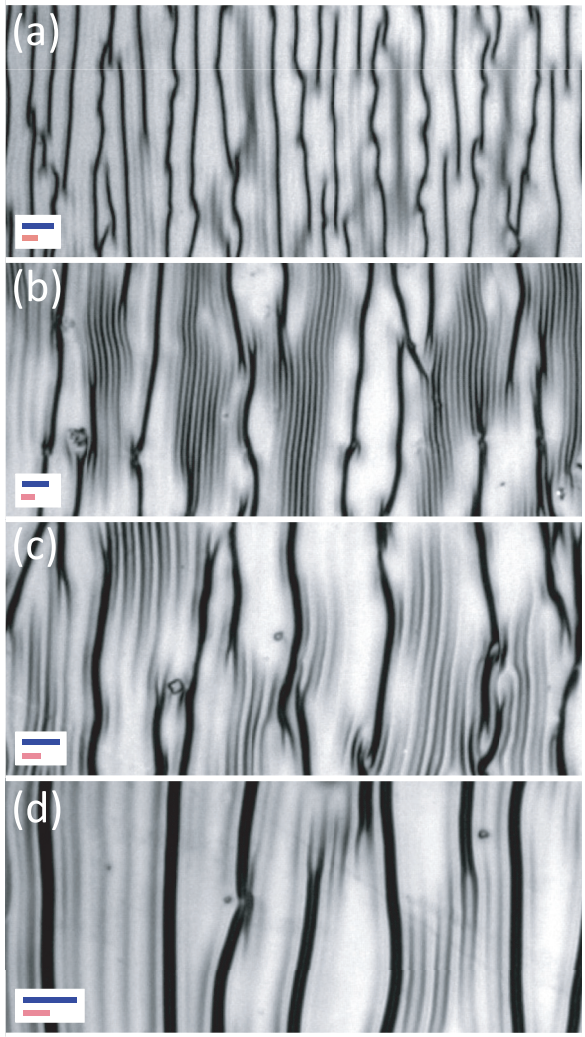

FIG. 3. (Color online) PS films compressed at 5% strain on PDMS at (a) $h = 35$ nm, (b) 50 nm, (c) 80 nm, and (d) 130 nm. The red (light) bar is the measured λ_0, the blue (dark) bar is twice this, and the width of each image is 110 μm. The darkest features are "folds" or crests.

Figure 5(d) shows the location of the λ_0, $2\lambda_0$, and $4\lambda_0$ peaks in $c(x)$ as a function of mean film thickness. All of the peak positions scale linearly with h, which is anticipated. Physically, when ξ is larger than both λ_0 and $2\lambda_0$, the dominant neighboring fold is forced to $4\lambda_0$ to accommodate the disorder but still be commensurate with a multiple of $2\lambda_0$. A state diagram in the plane of mean sample thickness (h) and strain (ϵ) is shown in Fig. 5(e). The circles in the region at the left denote pure harmonic ($1x$) wrinkling, the middle triangles indicate localization behavior with $4x$ mean spacing, and the squares in the region at the right indicate localization with $2x$ mean spacing. The dashed lines indicate the approximate locations of transitions. Pure harmonic (λ_0) wrinkling is only favored at small strains and thicker films, with doubling emerging at larger strains for all thicknesses. In between, at moderate strains, $4x$ behavior is favored. It is important to note, however, that harmonic wrinkling always coexists with the other two types of behavior. An example of $c(x)$ measured in the doubling region is shown in Fig. 5(f), where λ_0 is around 2 μm.

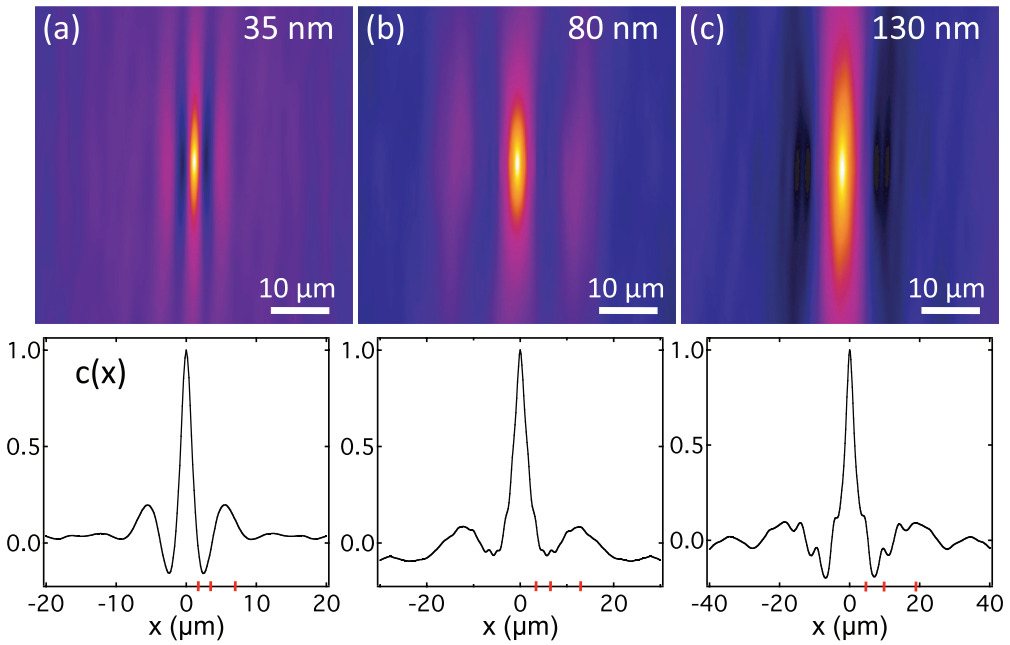

FIG. 4. (Color online) Correlation function $c(\mathbf{r})$ for the images in Fig. 3, with the x-projection, $c(x)$, in the bottom panel. The red hatch marks on the x-axis indicate λ_0, $2\lambda_0$, and $4\lambda_0$.

The measurements in Fig. 5 suggest that the disorder has the largest impact for thinner films (where $\delta h/h$ will be largest in magnitude) and larger strains, since this is the region of Fig. 5(e) where the $4x$ and $2x$ behavior emerges. We should note, however, that the region of the state diagram labeled as "$1x$" also exhibits long-wavelength folding, but typically at length scales much larger (6 to 12 times) than λ_0. In this view, disorder always has a measurable impact on the films, but length-scale doubling becomes more prominent at larger strains. Again, the fact that the $2x$ behavior crosses over to $4x$ behavior with *decreasing* strain at modest strains implicates disorder and not some other nonlinear effect commonly studied for homogeneous elastic films, which would predict progressive bifurcations emerging at progressively higher strains [15,19].

C. Single-wall carbon nanotubes

Thin films of single-wall carbon nanotubes (SWCNTs) have potential applications as transparent conductive coatings and p-type semiconducting layers in electronic and photovoltaic devices. Applications with mechanical flexibility are particularly well suited to these polymer-like materials, but pristine SWCNT films can be inherently unstable in response to certain types of deformation [31–33]. By depositing SWCNT coatings of varied thickness on pre-stretched PDMS substrates, the deformation mechanics has been studied as a function of SWCNT length, electronic type, film thickness, and strain [31–33]. These experiments are consistent with a pristine coating that has a remarkably high plateau modulus—reflecting the 1 TPa Young modulus of an individual SWCNT—but a very small yield strain. Compression pushes the SWCNTs into van der Waals bundles perpendicular to the direction of strain, which is the source of the plasticity [34].

Light scattering suggests that these films are "fractal" [31–33], and this inhomogeneity is reflected in the wrinkling pattern that emerges in response to strain [Figs. 6 and 7(a)], which bears a striking resemblance to the patterns exhibited by the disordered PS films in the previous section. The SWCNT films also exhibit significant fluctuations in thickness over a broad range of length scales, from the nanoscale up to the macroscale, as shown in Fig. 7(b), and by analogy with the experimental results for PS in the previous section, we can thus expect a mean spacing of either $2\lambda_0$ or $4\lambda_0$. A typical comparison of half of the measured wavelength [red/light bars, Fig. 7(b)] with the corresponding variations in thickness suggests that there are strong variations in h on the scale of wrinkling.

The use of Eq. (1) overestimates the plateau modulus of the films, putting it above the modulus of an individual nanotube (a physical impossibility). Previous studies thus analyzed such data based on Eq. (2), where "wavelength" doubling was qualitatively attributed to thickness fluctuations [31,32]. Figure 7(c) shows the typical behavior of the plateau modulus as a function of percolation depth and Fig. 8 shows the strain dependence of the modulus, which shows power-law strain softening at larger strains. The simple constitutive relation $E(\epsilon) = E_0(1 + \epsilon/\epsilon_0)^{-\alpha}$ has been used here (in combination with a small background) to model the strain dependence shown in Fig. 8, where the motivation for this expression in the context of purified SWCNT networks is given in Refs. [31] and [32]. Previous studies suggest that as the modulus increases, the yield strain decreases, and typical values of the exponent α are around 2 to 2.5 [31,32,34]. For complex fluids in general, this type of strain dependence has recently been used, for example, to model the nonlinear rheology of power-law gels [35], while analogous yield-strain behavior has been observed in glassy colloids [36].

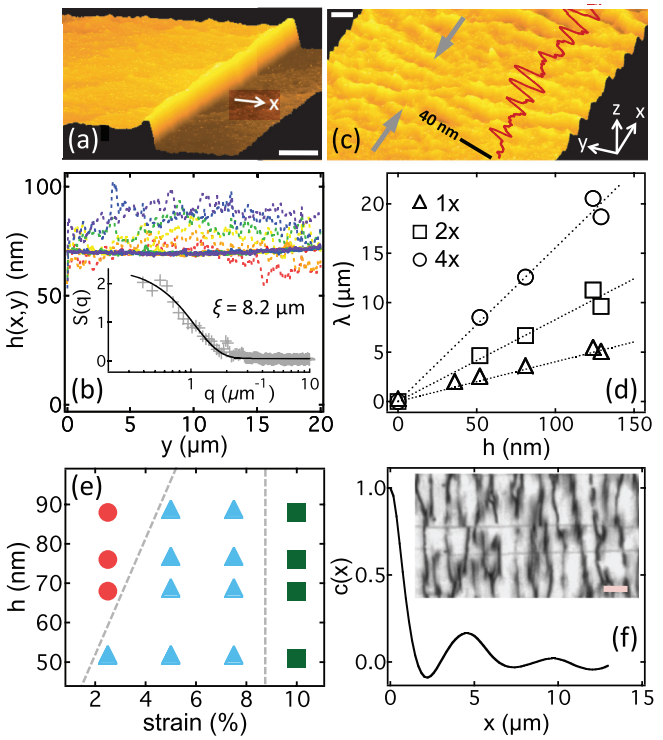

FIG. 5. (Color online) (a) AFM image near the edge of a PS film on unstrained PDMS (2.5 μm scale) and (b) height fluctuations obtained from AFM projections (at 2 μm intervals) for PS on silicon (solid) and PS on unstrained PDMS (dashed). The inset is $S(q)$ for film roughness on PDMS with a Gaussian fit. (c) AFM image of a wrinkled PS film on PDMS at 1% strain (2.5 μm scale) with a typical projection (red/dark). (d) Peak position vs thickness for the $1x$, $2x$, and $4x$ features at 5% strain. (e) "State diagram" in the plane of h and ϵ, where the markers denote the morphologies described in the text. (f) Measured $c(x)$ for $h = 50$ nm at 10% strain, where $\lambda_0 = 2$ μm. The inset is an optical image (5 μm scale).

A physical value for the plateau modulus of a nanotube film can be estimated from the theoretical work of Cox on 2D fiber networks in the absence of a matrix, which gives $E_0 \simeq E_{\rm tube}\phi/3$ where ϕ is the effective volume fraction of nanotubes [37]. The data in Fig. 8 correspond to a SWCNT film of mean thickness 22 nm and a surface mass density of 1 μg/cm^2 assembled from length-purified CoMoCat nanotubes of mean

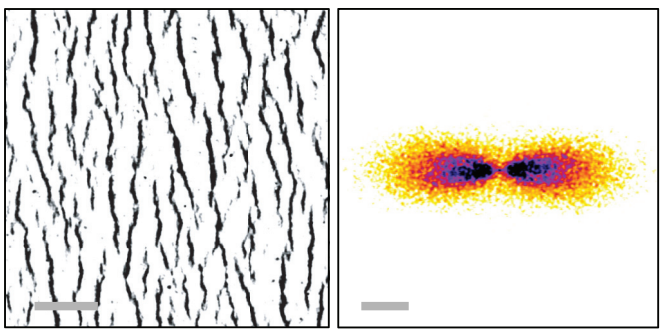

FIG. 6. (Color online) Wrinkling in a compressed SWCNT film on PDMS (left, 3 μm scale, 2.5% strain) and the corresponding digital power spectrum (right, 2 μm^{-1} scale).

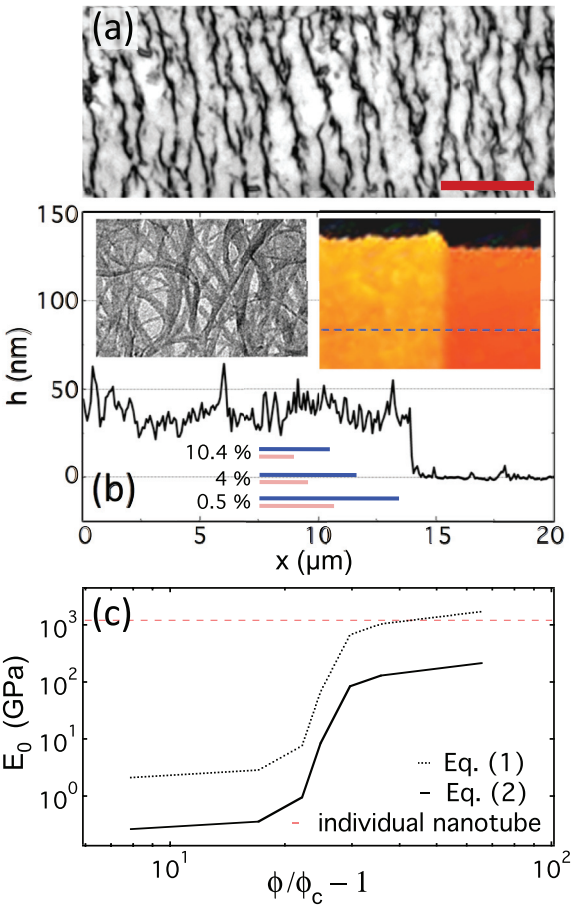

FIG. 7. (Color online) (a) Optical image of wrinkling in a SWCNT film of thickness 35 nm at 5% strain (20 μm scale). (b) Height of an unstrained nanotube film on quartz, with the corresponding AFM image (right inset, 3 μm width) and a typical TEM image (left inset, 500 nm width). The blue/dark bars are the measured wrinkling length scale at the indicated strain and the red/light bars are half this. (c) Plateau modulus based on Eqs. (2) (solid) and (1) (dashed) with the modulus of a nanotube (red/light).

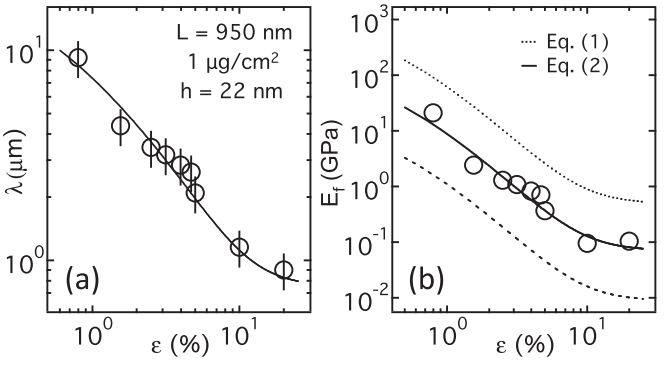

FIG. 8. (a) Wavelength as a function of strain and (b) modulus as a function of strain for a SWCNT film. Data are from Ref. [32] and the fit is based on Eq. (2) with a strain-softening modulus as described in the text. The upper dashed curve represents the overestimate obtained from Eq. (1) and the lower dashed curve represents the underestimate obtained assuming wavelength quadrupling ($\lambda_0 \to 4\lambda_0$).

length 950 nm, for which the effective volume fraction is $\phi \simeq 0.5$ and $E_{\text{tube}} \simeq 1$ TPa [31,32]. This gives the estimate $E_0 \simeq 180$ GPa, while the fit in Fig. 8 gives $E_0 \simeq 200$ GPa and $\epsilon_0 \simeq 0.4\%$, in reasonable agreement. Using Eq. (1), in contrast, gives the unphysical value $E_0 \simeq 1.6$ TPa, while assuming an average spacing of $4\lambda_0$ gives the underestimate $E_0 \simeq 25$ GPa.

III. INHOMOGENEOUS FILMS

We suggest that the physical origin of folding and length-scale doubling in disordered films on soft substrates resides mainly in two effects. The first is the tendency for "defects" (such as strong or weak points associated with thickness fluctuations) to either locally enhance (for smaller local thickness) or locally suppress (for larger local thickness) the deformation $u(x)$. Starting conceptually from a homogeneous compressed film under harmonic deformation, the random addition of more than one defect (in the form of a thickness fluctuation or a quenched variation in modulus) will frustrate the periodicity of the harmonic pattern such that the only option for the film is to localize the deformation around the defects, which gives rise to the characteristic pattern in the figures.

The second effect is how these localization sites interact with one another. The deformation of a compressed film is a balance of film bending and substrate stretching, and a derivation of Eq. (1) is given in supporting Supplemental Material [38]. Since the substrate stretching is proportional to the deformation $u(x)$, the magnitude of the stress-stress correlation function can be simply approximated by the correlation function $c(x)$, which in Figs. 4 and 5(f) has a sharp cutoff at $x = \lambda_0$ and a secondary peak at $x = 2\lambda_0$. Since the stress must be distributed as uniformly as possible, regions of localization cannot overlap within the width of their stress correlation. Another way of stating this is that the "packing" of localization sites (folds) is dictated by the width of their stress correlation function. Based on the correlation lengths λ_0 and $2\lambda_0$, strongly interacting folds (those that approach up to the central cutoff λ_0) will thus have a disordered (as opposed to periodic) arrangement dictated by the distribution of defects, but with a mean spacing of twice the cutoff ($2\lambda_0$). Weakly interacting folds (those that approach to within the first peak in the stress correlation function) will exhibit twice this mean spacing, or $4\lambda_0$. The scenario is shown schematically in Fig. 9, where the interacting profiles can equally represent either localized folds or stress correlation functions.

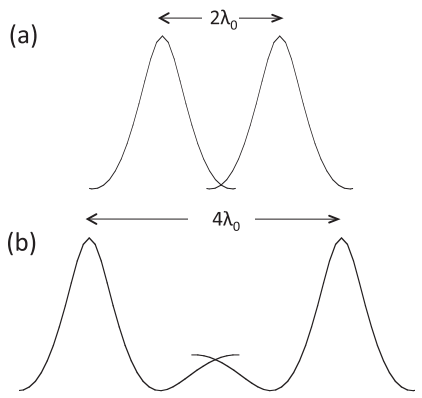

FIG. 9. (a) Relative spacing of folds when the width of the stress-stress correlation function is $2\lambda_0$, and (b) when the width of the stress-stress correlation function is $4\lambda_0$.

IV. CONCLUSIONS

Wrinkling in three specific types of disordered films on elastic substrates has been examined experimentally at small strains, revealing a disordered pattern with a nonperiodic arrangement of localized folds. The two elastic films (diblock copolymers and glassy polymers) show clear doubling of the characteristic length scale—and in certain instances even quadrupling—with respect to a homogeneous film of comparable modulus, while a "plastic" or strain-softening film (SWCNTs) shows the same disordered pattern in a manner consistent with length-scale doubling. Qualitatively, we attribute these observations to (i) localized deformation triggered by structural inhomogeneities that frustrate the underlying harmonic deformation, and (ii) the subsequent interaction of neighboring folds or localization sites through their local stress distribution. We suggest that adjacent folds can only approach each other within the width of their stress-stress correlation function. If the width of the stress correlation function is $2\lambda_0$, the average spacing of folds will be $2\lambda_0$. Conversely, if the folds can interact at longer length scales through the secondary peak in the stress correlation function, the mean spacing of folds will be $4\lambda_0$.

While the fact that these patterns are observed at small strains would seem to suggest that material nonlinearity is not important, care should be taken, since the strong deformation implicit to localization might imply that nonlinear effects could be required to quantitatively account for the profile $u(x)$ with a 1D model. We are currently working on a nonlinear model of film wrinkling that accounts for this type of disorder. The experimental evidence we offer here, however, suggests that polystyrene, which has a well-characterized plane-strain modulus and exhibits both harmonic wrinkling and localization, can serve as a useful reference point for characterizing the wrinkling of disordered films comprised of more complex and poorly understood materials.

Our results have important implications for measuring the mechanical properties of disordered thin films on elastic substrates through the spatial and topographical distribution of the surface features that emerge under compression. Since $1x$ (harmonic) behavior always appears to be present in an elastic film, care should be taken to count all the features independent of amplitude before using Eq. (1). The familiar result for homogeneous or harmonic wrinkling should then only be used for regions that show clear harmonic deformation. Otherwise, the $2x$ model [Eq. (2)] should be used, with the constraint that the modulus should be a smooth function of strain. This will ensure that the results are not being biased by the emergence of $4x$ behavior at small strains, which would cause the modulus to appear artificially high by a factor of 2^3.

We suggest that for "plastic" or strain-softening films, localized structural failure will prevent the type of long-range fold-fold interactions that appear to give rise to the intermediate $4x$ behavior observed in disordered elastic films. Schematically, the scenario in Fig. 9(a) would be favored over that depicted in Fig. 9(b) for a strain-softening film, since

localization of the deformation can trigger plastic structural changes that could diminish the ability of the folds to interact at longer scales [31,32]. Based on the observations reported in Sec. II B for PS films, it is reasonable to ask if the SWCNT films would be better interpreted assuming $4x$ behavior. This can be addressed through the results presented in Sec. II C. At the highest strain of 20% in Fig. 8(b), an analogy with the PS films suggests that we should assume $2x$ behavior for any easily discernible structure. If a transition to $4x$ behavior were to then occur below 10% in Fig. 8(b), as it does for PS in Fig. 5(e), the strain-dependent modulus would exhibit a discontinuous drop below 100 MPa with decreasing strain, which would be unphysical. In addition, the extrapolated low-strain modulus would then be too small to be reconciled with the 1 TPa modulus of an individual nanotube.

Given the emerging importance of thin films and coatings assembled from purified nanoparticles [39], and in light of the similarities we demonstrate here between the morphology of wrinkling in disordered polymer films and thin nanotube films, a better theoretical understanding of the influence of quenched disorder on the mechanics of wrinkling, folding and localization is clearly warranted. We hope that the experimental insights offered here will help guide such efforts. Another interesting and relevant question, particularly for SWCNT films, is the role of viscoelasticity, which has recently emerged as a topic of potential importance [40,41]. In the present study, we have tried to limit the influence of such effects by always releasing the strain at the same rapid rate, but future experiments will address the question of rate dependence in greater detail.

ACKNOWLEDGMENTS

A.B.C. gratefully acknowledges the support of the National Science Foundation (NSF) through grant no. EPS-0814442 and E.K.H. gratefully acknowledges the support of the NSF through grant no. CMMI-0969155. We also thank Daniel M. Kroll for critical insight and helpful discussions.

[1] M. Trejo, C. Douarche, V. Bailleux, C. Poulard, S. Mariot, C. Regeard, and E. Raspaud, Proc. Nat. Acad. Sci USA **110**, 2011 (2013).
[2] M. Kücken and A. C. Newell, J. Theo. Biol. **235**, 71 (2005).
[3] T. Ohzono and Hirosato Monobe, J. Coll. Int. Sci. **368**, 1 (2012).
[4] M. Ramanathan, B. S. Lokitz, J. M. Messman, C. M. Stafford, and S. M. Kilbey, J. Mater. Chem. C **1**, 2097 (2013).
[5] E. Cerda and L. Mahadevan, Phys. Rev. Lett. **90**, 074302 (2003).
[6] C. M. Stafford, C. Harrison, K. L. Beers, A. Karim, E. J. Amis, M. R. Vanlandingham, H.-C. Kim, W. Volksen, R. D. Miller, and E. E. Simonyi, Nat. Mater. **3**, 545 (2004).
[7] J. Huang, M. Juszkiewicz, W. H. de Jeu, E. Cerda, T. Emrick, N. Menon, and T. P. Russell, Science **317**, 650 (2007).
[8] N. Bowden, S. Brittain, A. G. Evans, J. W. Hutchinson, and G. M. Whitesides, Nature **393**, 146 (1998).
[9] E. P. Chan, E. J. Smith, R. C. Hayward, and A. J. Crosby, Adv. Mater. **20**, 711 (2008).
[10] E. Sultan and A. Boudaoud, J. Appl. Mech. **75**, 051002 (2008).
[11] X. Chen and J. W. Hutchinson, J. Appl. Mech. **71**, 597 (2004).
[12] J. Genzer and J. Groenewold, Soft Matter **2**, 310 (2006).
[13] H. Jiang, D. Khang, J. Song, Y. Sun, Y. Huang, and J. A. Rogers, Proc. Natl. Acad. Sci. **104**, 15607 (2007).
[14] J. Yin and X. Chen, J. Phys. D: Appl. Phys. **44**, 045401 (2011).
[15] J.-Y. Sun, S. Xia, M.-Y. Moon, K. H. Oh, and K.-S. Kim, Proc. R. Soc. London, Ser. A **468**, 932 (2012).
[16] R. Huang, J. Mech. Phys. Solids **53**, 63 (2005).
[17] J. Song, H. Jiang, Z. J. Liu, D. Y. Khang, Y. Huang, J. A. Rogers, C. Lu, and C. G. Koh, Int. J. Solids Struct. **45**, 3107 (2008).
[18] B. Audoly and Y. Pomeau, *Elasticity and Geometry* (Oxford University Press, Oxford, 2010).
[19] F. Brau, H. Vandeparre, A. Sabbah, C. Poulard, A. Boudaoud, and P. Damman, Nat. Phys. **7**, 56 (2011).
[20] T. A. Witten, Rev. Mod. Phys. **79**, 643 (2007).
[21] L. Pocivavsek, R. Dellsy, A. Kern, S. Johnson, B. Lin, K.-Y. C. Lee, and E. Cerda, Science **320**, 912 (2008).
[22] B. Davidovitch, R. D. Schroll, D. Vella, M. Adda-Bedia, and E. A. Cerda, Proc. Nat. Acad. Sci. USA **108**, 18227 (2011).
[23] H. Diamant and T. A. Witten, Phys. Rev. Lett. **107**, 164302 (2011).
[24] B. Audoly, Phys. Rev. E **84**, 011605 (2011).
[25] T. Tallinen, J. A. Astrom, and J. Timonen, Nat. Mater. **8**, 25 (2009).
[26] B. J. Gurmessa and A. B. Croll, Phys. Rev. Lett. **110**, 074301 (2013).
[27] D.-P. Holmes and A. J. Crosby, Phys. Rev. Lett. **105**, 038303 (2010).
[28] Y. Ebata, A. B. Croll, and A. J. Crosby, Soft Matter **8**, 9086 (2012).
[29] A. B. Croll and A. J. Crosby, Macromolecules **45**, 4001 (2012).
[30] F. S. Bates and G. H. Fredrickson, Annu. Rev. Phys. Chem. **41**, 525 (1990).
[31] E. K. Hobbie, D. O. Simien, J. A. Fagan, J. Y. Huh, J. Y. Chung, S. D. Hudson, J. Obrzut, J. F. Douglas, and C. M. Stafford, Phys. Rev. Lett. **104**, 125505 (2010).
[32] J. M. Harris, G. R. S. Iyer, D. O. Simien, J. A. Fagan, J. Y. Huh, J. Y. Chung, S. D. Hudson, J. Obrzut, J. F. Douglas, C. M. Stafford, and E. K. Hobbie, J. Phys. Chem. C **115**, 3973 (2011).
[33] J. M. Harris, G. R. S. Iyer, A. K. Bernhardt, J. Y. Huh, S. D. Hudson, J. A. Fagan, and E. K. Hobbie, ACS Nano **6**, 881 (2012).
[34] E. K. Hobbie, T. Ihle, J. M. Harris, and M. R. Semler, Phys. Rev. B **85**, 245439 (2012).
[35] T. S. K. Ng and G. H. McKinley, J. Rheol. **52**, 417 (2008).
[36] V. Kobelev and K. S. Schweizer, Phys. Rev. E **71**, 021401 (2005).
[37] H. L. Cox, Br. J. Appl. Phys. **3**, 72 (1952).
[38] See Supplemental Material at http://link.aps.org/supplemental/10.1103/PhysRevE.88.032409 for a derivation of Eq. (1) in the general case of a homogeneous strain-softening film.
[39] J. B. Miller and E. K. Hobbie, J. Polym. Sci. Part B: Polym. Phys. **51**, 1195 (2013).
[40] E. P. Chan, K. A. Page, S. H. Im, D. L. Patton, R. Huang, and C. M. Stafford, Soft Matter **5**, 4638 (2009).
[41] P. A. O'Connell, G. B. McKenna, E. P. Chan, and C. M. Stafford, Soft Matter **7**, 788 (2011).